Electronic Supplementary Material (ESI) for Journal of Materials Chemistry C.

Supporting Information

Competing thermal expansion mismatch and lattice strain engineered growth of crack free WS_2 in-plane heterostructures

[1]Pawan Kumar, [2]Birender Singh, [2]Pradeep Kumar and [1]Viswanath Balakrishnan*

[1]School of Engineering, Indian Institute of Technology Mandi, Kamand, Himachal Pradesh-175005, India.

[2]School of Basic Sciences, Indian Institute of Technology Mandi, Kamand, Himachal Pradesh-175005, India.

* Corresponding author, E-mail: viswa@iitmandi.ac.in

Structure of 1T, 1H and 1T' phases in WS_2:

WS_2 has mainly three allotropes in its structure which are 1T, 1H and 1T' depending on coordination of S-atom with W-atoms as well as stacking order of its layers. Among the three polymorphs, 1H having trigonal prismatic coordination while 1T and 1T' have commonly octahedral coordination. Formation of two polytypes next to each other is trivial with coexisting phase materials and stabilizing themselves resulting from the thermodynamic favored conditions. Strain energy minimization stabilizes co-existing phases at room temperature and has been explored here upto their decomposition states using in-situ PL measurements.

S. No.	2D Layer	Phase	Space Group	Structure (Co-ordination)	Lattice Parameters		Band Gap
1.	MoS_2	1T	$P\bar{3}m1$	Trigonal (Octahedral)	a=5.6Å	c=5.99Å	Metallic
2.		1T'		Trigonal (Octahedral)			Semi-metallic
3.		1H		Hexagonal(Trigonal prismatic)			Semiconducting
4.		2H	$P6_3/mmc$ D_{6h}:$P\bar{6}m2$ D_{3h}	Hexagonal(Trigonal prismatic)	a=3.15 Å	c=12.3Å	Semiconducting
5.		3R	R3m	Rhombohedral(Trigonal prismatic)	a=3.17 Å	c=18.38 Å	Semiconducting
6.		1T	$P\bar{3}m1$	Tetragonal(Octahedral)			Metallic

7.	WS_2	1T’		Trigonal(Octahedral)			Semi-metallic
8.		1H		Hexagonal			
9.		2H	$P6_3/mmc$	Hexagonal	a=3.19 Å		Semiconducting
10.		3R	R3m	Rhombohedral(Trigonal prismatic)	a=3.16 Å	c=18.5 Å	Semiconducting

Physical and chemical properties in bulk polytype of 1H and 1T’ are almost equal except its slightly changed band structure. 1H polytype show semiconducting in nature while 1T and 1T’ show metallic and semimetallic, both form due to distortions in coordination geometry. This causes slight changes in PL position (1H and 1T’) with slightly reduced intensity. While the metallic 1T phase known to show complete PL quenching, the observed 1T’ phase shows considerable intensity due to its semimetallic in nature.

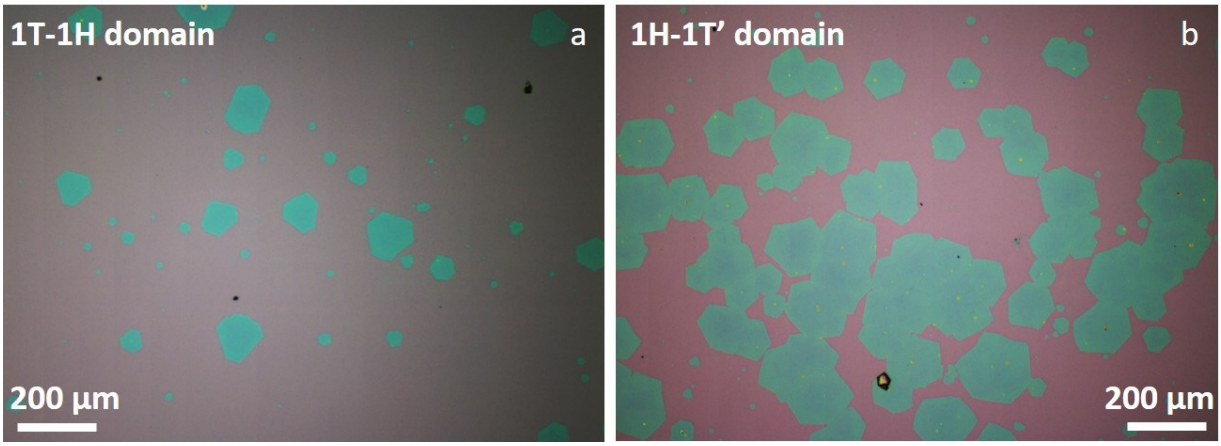

Figure S1: VLM image of monolayer WS_2 with wide dispersion of large areal flakes for (a) 1T-1H phase as well as (b) 1H-1T’ phase respectively. Here we could see no optical contrast for coexisting phases present in as grown monolayers.

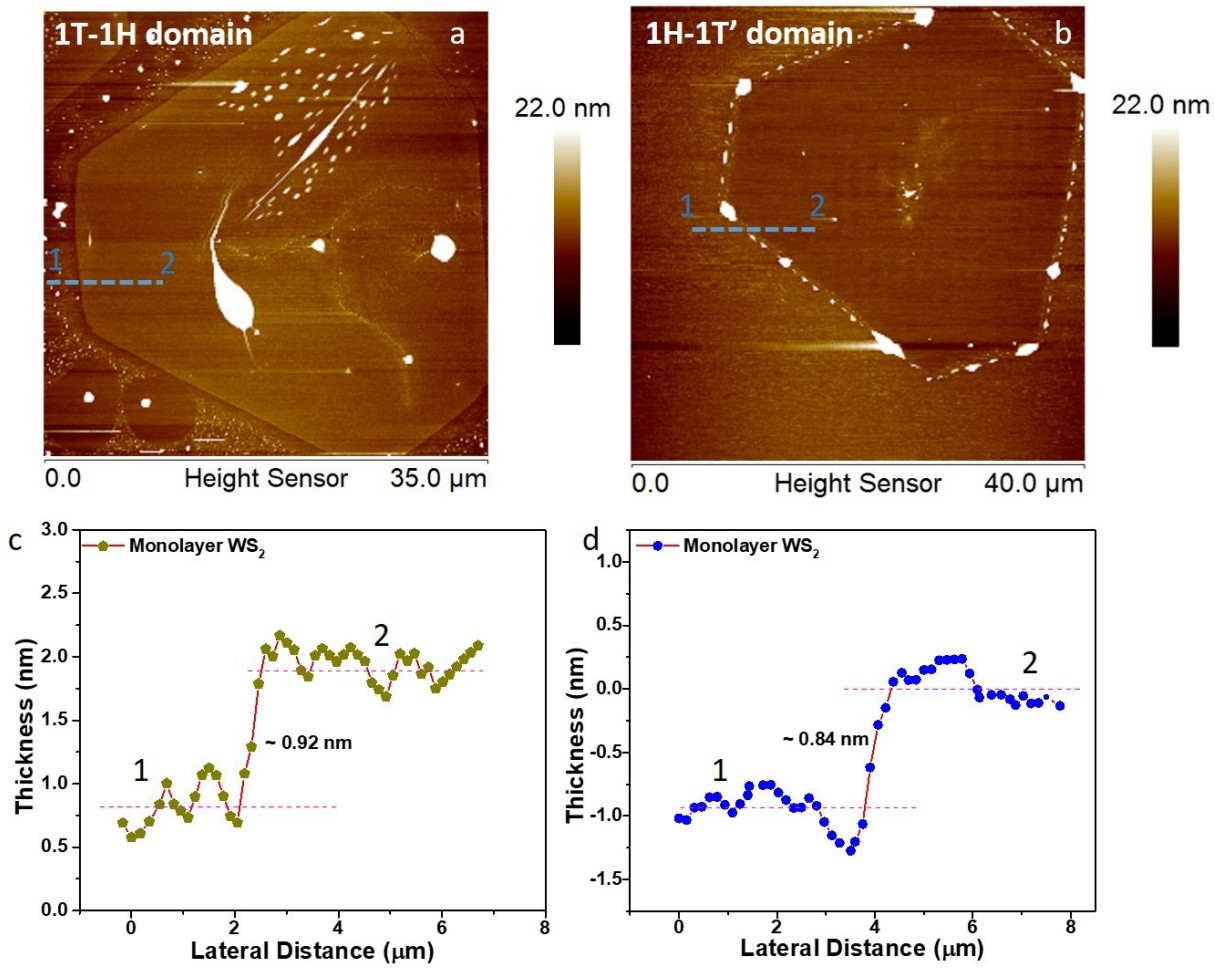

Figure S2: Surface morphology and thickness profile of as grown monolayers are characterized using atomic force microscopy (AFM). (a, b) Representative AFM height image and thickness profiling (c, d) of as grown monolayer WS_2 with coexisting 1T-1H and 1H-1T' polymorphs respectively.

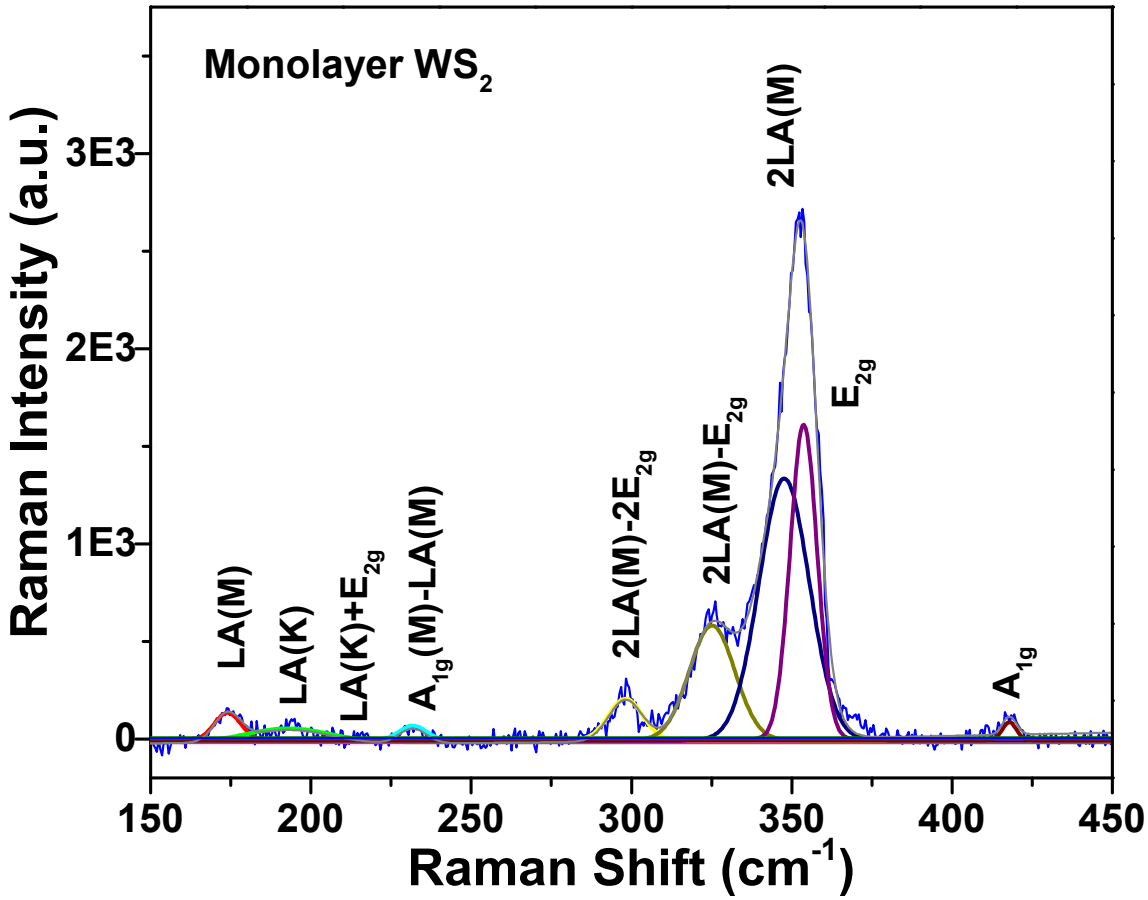

Figure S3: Basic indexing for as present all Raman modes in 1H monolayer WS_2.

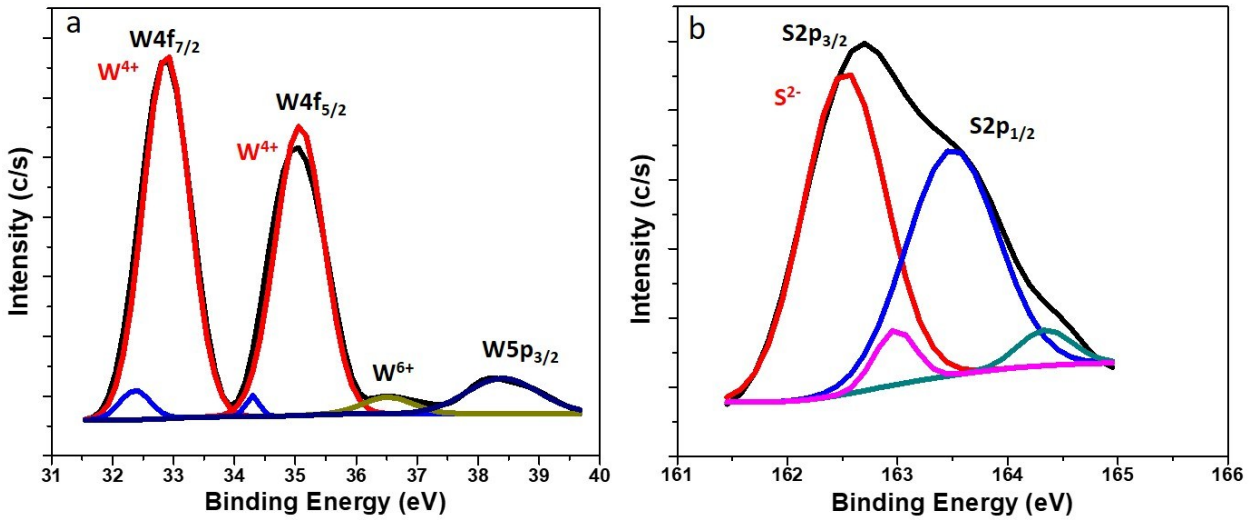

Figure S4: XPS characteristics of monolayer WS_2 with W and S-oxidation states which corresponds to formation of WS_2 along with small amount of Oxygen presence (W^{6+}) which might be cause of O_2-adsorption at monolayer active edges from atmosphere.

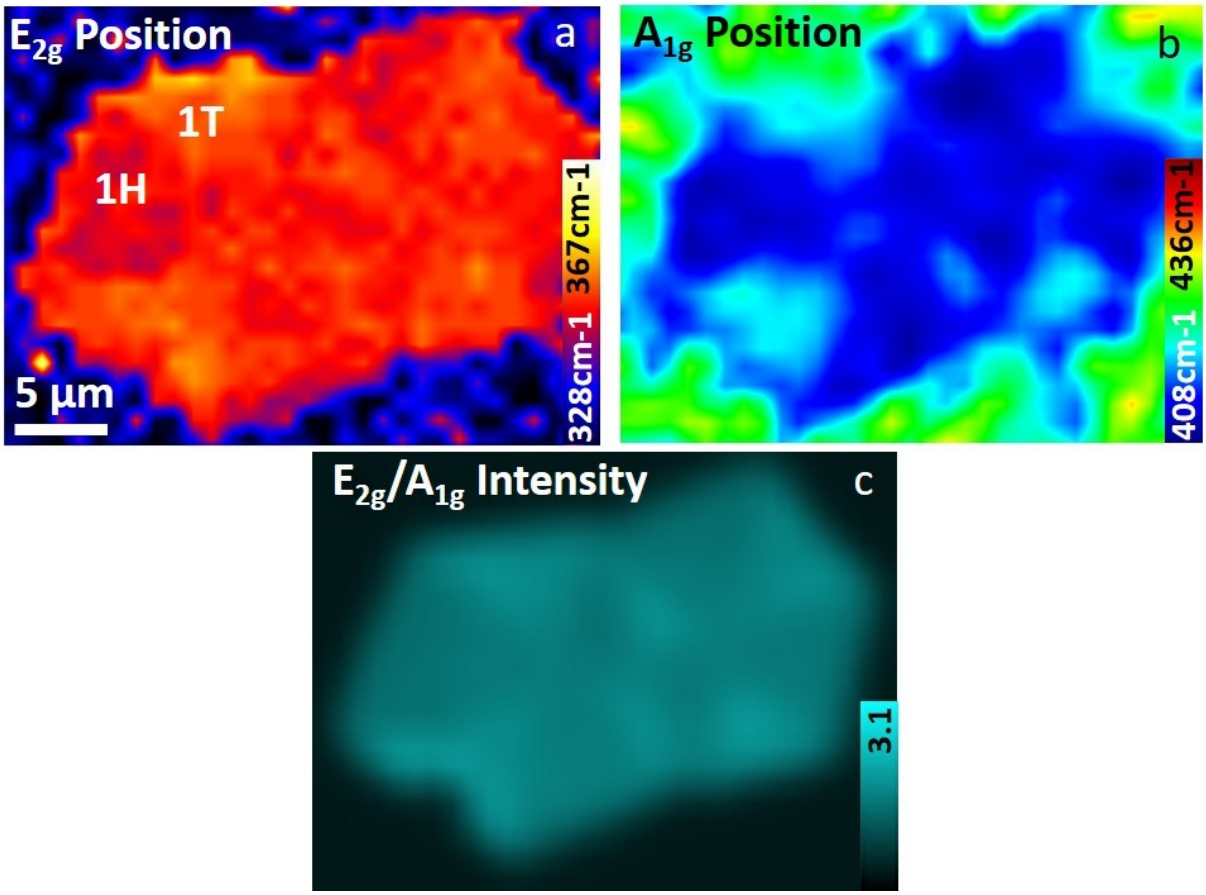

Figure S5: Spatially resolved Raman position mapping for 1T-1H polymorph of monolayer WS_2 which coexist in a single domain as indicated here and shown for E_{2g}, A_{1g} positions as well as their ratio intensity mapping.

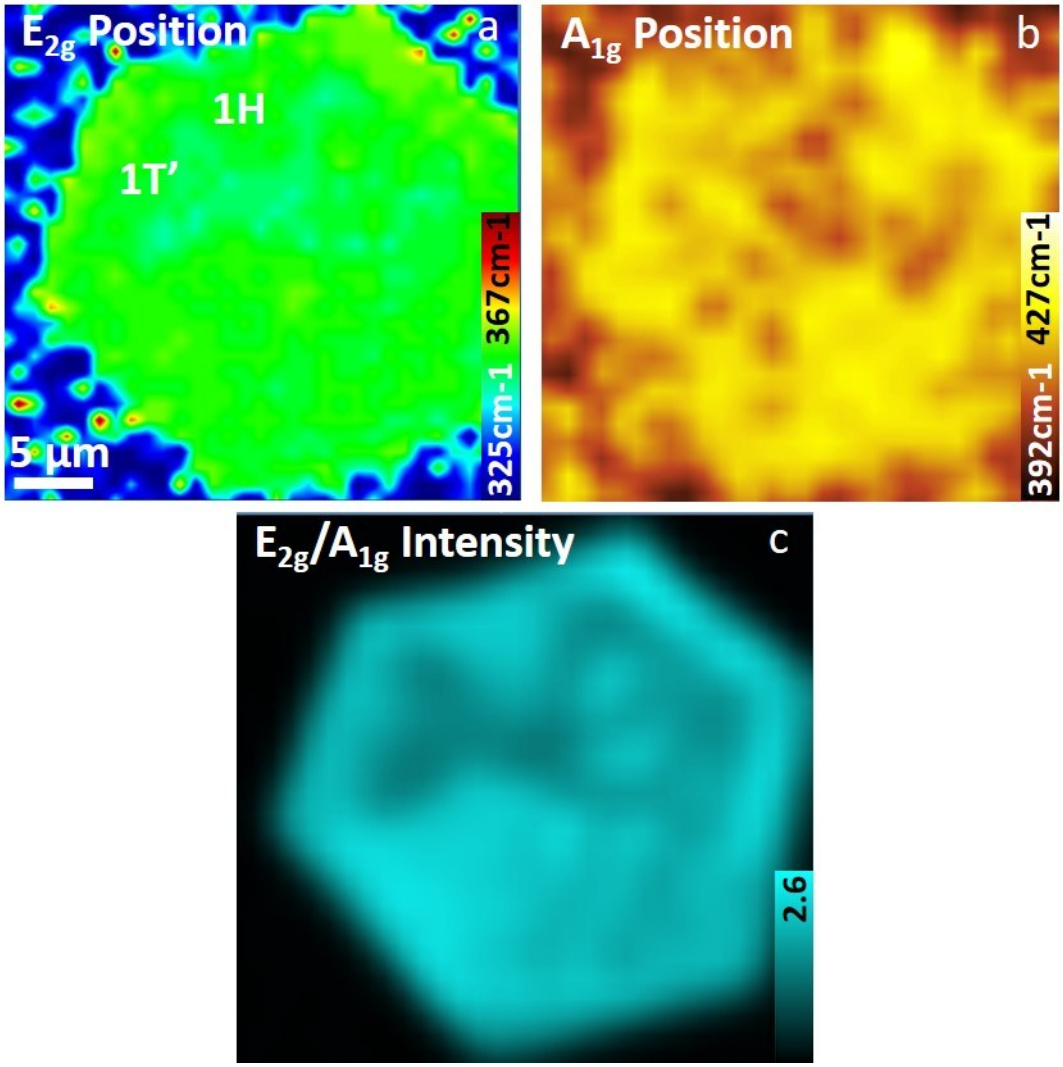

Figure S6: Spatially resolved Raman position mapping for 1H-1T' polymorph of monolayer WS_2 which coexist in a single domain as indicated here and shown for E_{2g}, A_{1g} positions as well as their ratio intensity mapping.

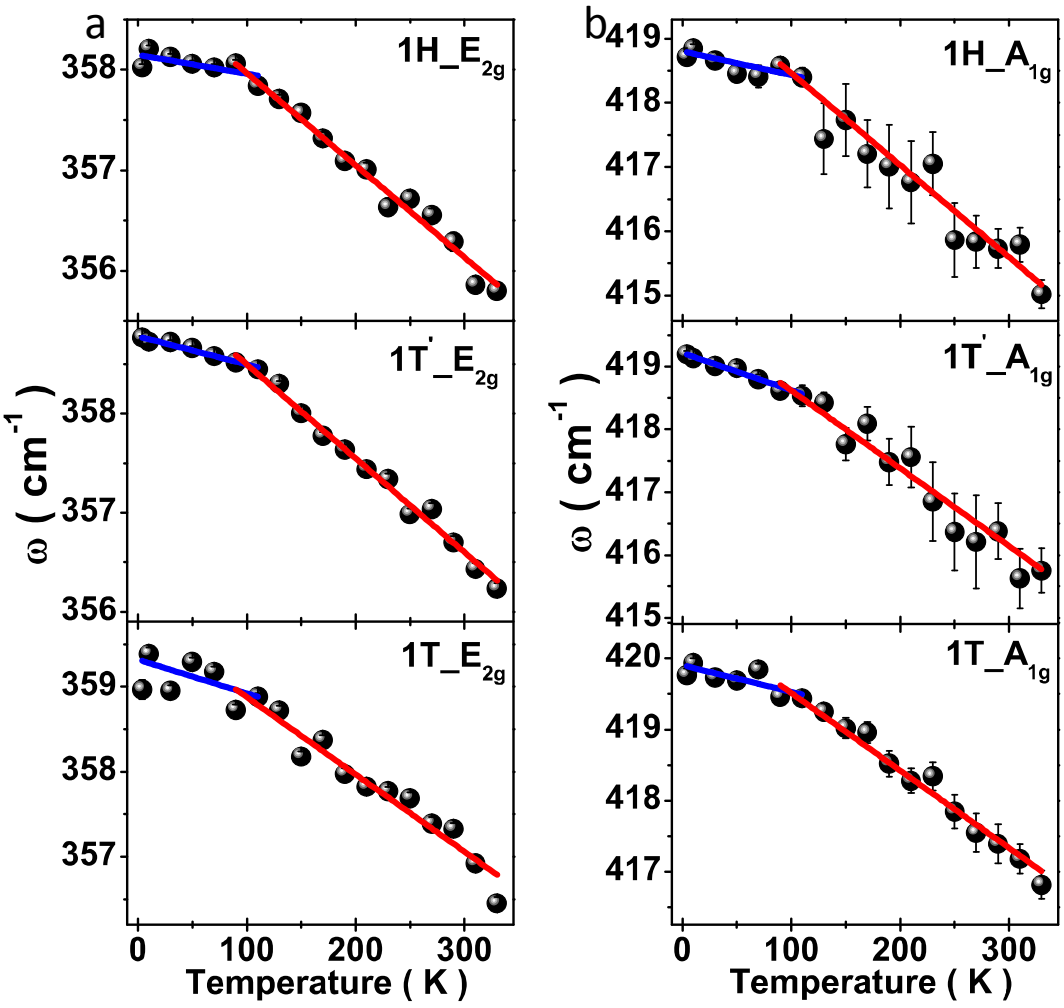

Figure S7. Linearly Fitted E_{2g} and A_{1g} modes for 1T, 1H and 1T' polymorphs of monolayer WS_2 are shown in (a) and (b) for temperature range of 4K-330K respectively. Two fitting regions have been identified as 4K-110K and 110K-330K respectively for which it suited well for linear variation of in-plane (E_{2g}) and out of plane (A_{1g}) modes.

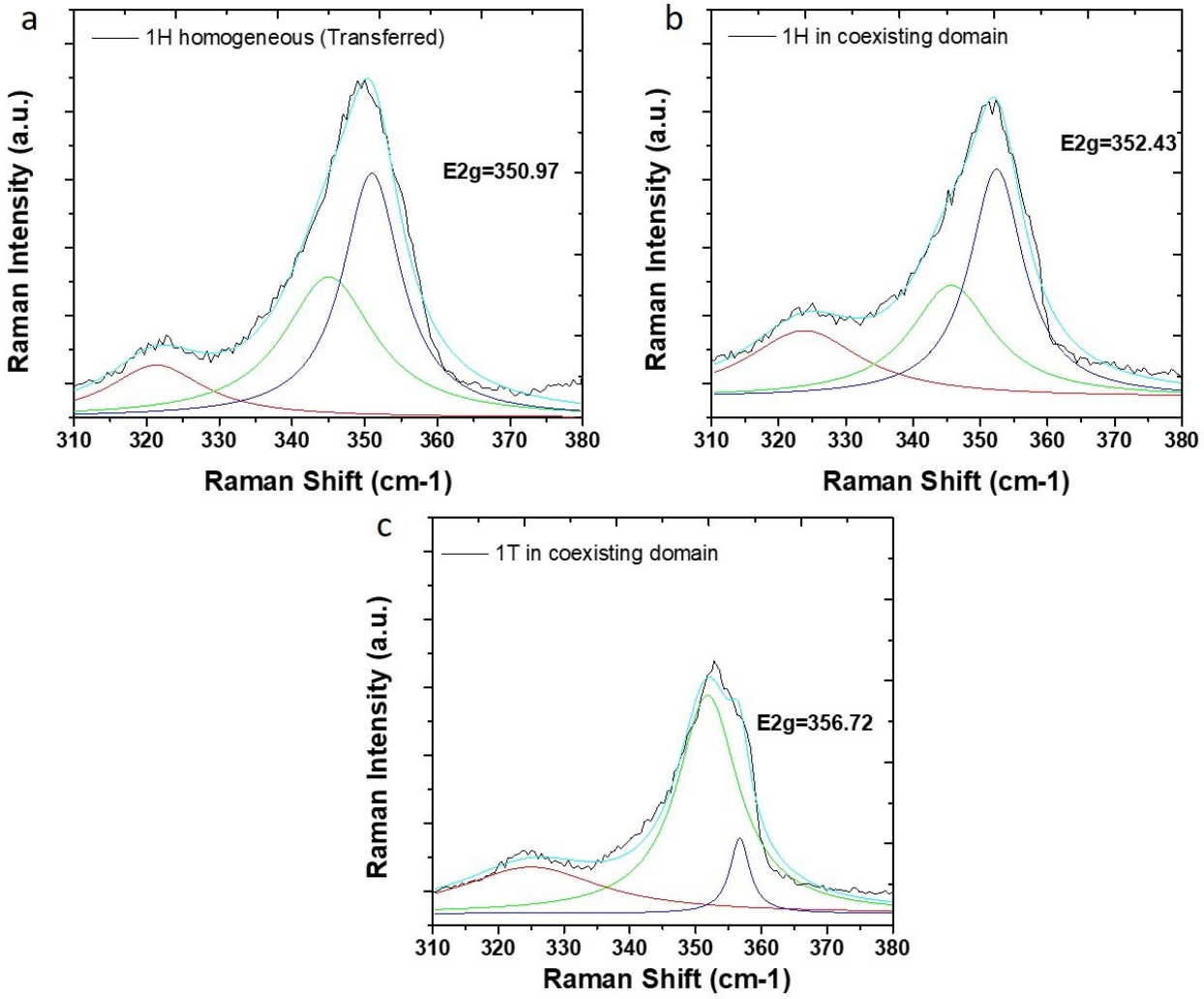

Figure S8: Deconvoluted Raman band for 2LA (M) and E_{2g} band for monolayer WS_2 to distinguish Raman shift between (a) homogeneous (1H only), (b) 1H heterogeneous and (c) 1T heterogeneous phases.

Table ST1: Calculated parameters used to fit in three-phonon process and adapted model (equation 3 and 4) which suited to best to fit the nonlinearity of thermal expansion for 1H, 1T' and 1T phase of monolayer WS_2 using E_{2g} and A_{1g} modes respectively.

Phase	E_{2g}			
	c	**a_0**	**a_1**	**a_2**
1H	- (0.314 ± 0.043)	- (6.693 ± 4.023) x 10^{-6}	(2.360 ± 0.668) x 10^{-7}	- (4.862 ± 2.339) x 10^{-10}
1T'	- (0.155 ± 0.026)	- (2.261 ± 2.715) x 10^{-6}	(2.295 ± 0.466) x 10^{-7}	- (4.699 ± 1.652) x 10^{-10}
1T	- (0.109 ± 0.172)	(5.377 ± 6.559) x 10^{-6}	(1.356 ± 1.452) x 10^{-7}	- (1.995 ± 4.643) x 10^{-10}

Phase	A_{1g}			
	c	**a_0**	**a_1**	**a_2**
1H	- (1.276 ± 0.066)	(11.958 ± 7.845) x 10^{-6}	- (9.885 ± 5.538) x 10^{-8}	(5.449 ± 5.486) x 10^{-10}
1T'	- (0.877 ± 0.028)	(16.348 ± 3.602) x 10^{-6}	- (9.516 ± 7.836) x 10^{-8}	(4.994 ± 2.941) x 10^{-10}
1T	- (1.152 ± 0.062)	(11.768± 5.331) x 10^{-6}	- (9.811 ± 8.964) x 10^{-8}	(4.616 ± 3.095) x 10^{-10}